Computational and experimental studies on the catalytic mechanism of biliverdin IXβ reductase

Liam J Smith, Seamus Browne, Adrian J Mulholland, Timothy J Mantle

Computational and experimental studies on the catalytic mechanism of biliverdin IXβ reductase

Liam J.Smith[1], Seamus Browne[1], Adrian J. Mulholland[2] and Timothy J. Mantle[1]

School of Biochemistry and Immunology[1], Trinity College Dublin, Dublin 2, Ireland and Computational Chemistry Centre[2], School of Chemistry, University of Bristol, Cantock's Close, Bristol BS8 1TD, UK

Abstract

Biliverdin-IXβ reductase (BVR-B) also known as flavin reductase (FR) is a promiscuous enzyme catalysing the pyridine nucleotide dependent reduction of a variety of flavins, biliverdins, PQQ and ferric ion. Mechanistically it is a good model for biliverdin-IXα reductase (BVR-A), a potential pharmacological target for neonatal jaundice and also a potential target for adjunct therapy to maintain protective levels of biliverdin-IXα during organ transplantation. In a commentary [4] on the structure of BVR-B McDonagh (2001) noted one outstanding issue that remained was whether the mechanism was a concerted hydride transfer followed by protonation of a pyrrolic anion or protonation of the pyrrole followed by hydride transfer. We have attempted to address this question using quantum mechanics/molecular mechanics (QM/MM) calculations. QM/MM potential energy surfaces show that the lowest energy pathway proceeds with a positively charged pyrrole intermediate via two transition states. These initial calculations were performed with Histidine 153 as the source of the proton. However site directed mutagenesis studies with both the H153A and the H153N mutant reveal that His153 is not required for catalytic activity. We have repeated the calculation with a solvent hydroxonium donor and obtain a similar energy landscape indicating that protonation of the pyrrole is the most likely first step followed by hydride transfer and that the required proton may come from bulk solvent. The implications of this work for the design of inhibitors of BVR-A are discussed.

Introduction

The biological role of the linear tetrapyrroles biliverdin-IXα and bilirubin-IXα in mammalian systems remains unclear. Vertebrates, plants and cyanobacteria use structurally related haem oxygenases (HOs) to cleave the haem macrocycle to form the green "bile pigment" biliverdin-IXα (the transfer of reducing equivalents from NADPH to HO is via ferredoxin in plants and cyanobacteria [1] but via the flavoprotein cytochrome P450 reductase in mammals). The metabolic divergence occurs at the level of biliverdin-IXα. Plants and blue-green algae use biliverdin-IXα as a precursor for light sensing (phytochromobilin) and light harvesting (phycobilins) chromophores [2]. Mammals reduce biliverdin-IXα to bilirubin-IXα and the reaction is catalysed by biliverdin-IXα reductase [BVR-A] (the corresponding reaction catalysed by biliverdin-IXβ reductase is shown in Figure 1) generating an intermediate that is insoluble in aqueous solutions and which requires conjugation with glucuronic acid (this reaction is catalysed by the glucuronyltransferase UGT1A1) prior to excretion of the glucuronide into bile via the mrp2 organic anion pump [3]. In earlier literature, and more recently by McDonagh [4], the question has been raised "why convert biliverdin-IXα a non-toxic easily excretable waste product, into bilirubin-IXα, a substance that is unexcretable, neurotoxic, seeds gallstones and has to be further metabolised for disposal?"

In mammalian systems bilirubin plays a major role as a physiologically significant antioxidant although we are far from a complete understanding of this phenomenon. The haem catabolic pathway is currently receiving attention in a number of fields with the observation that induction of haem oxygenase-1 (HO-1) is cytoprotective [5, 6]. Attempts to relate this to production of the immediate product biliverdin-IXα [7, 8] and/or subsequent reduction to bilirubin-IXα [9] or to a redox cycling mechanism between these two linear tetrapyrroles [10] are unresolved. With regard to redox protection there is now good evidence [11] that low serum bilirubin-IXα is associated with a high risk of coronary artery disease (CAD). The corollary, that slightly elevated serum bilirubin-IXα is protective against CAD, has received support in studies showing that Gilberts patients (who have a less effective promoter for UGT1A1 and are therefore unable to conjugate bilirubin effectively with glucuronic acid) do not suffer from CAD [12, 13]. The antioxidant activity of bilirubin was first suggested to be of physiological significance by Ames and co-workers [14] although the mechanism remains unclear. Several reports have suggested that lipid hydroperoxides may be reduced to the corresponding alcohol and that bilirubin may be oxidised to biliverdin during this process. In model *in vitro* systems this reaction is not stoichiometric and clearly more work is needed to define this process *in vivo*. It has been proposed [10] that biliverdin-IXα and bilirubin-IXα are involved in a protective redox cycle where lipid hydroperoxide-linked oxidation of bilirubin-IXα to biliverdin-IXα is coupled with BVR-A maintaining protective levels of bilirubin-IXα. These conclusions were reached on the basis that cells knocked down for BVR-A mRNA are highly sensitive to H_2O_2 compared with control cells.

Mammals maintain relatively high levels of circulating bilirubin-IXα and excrete this in bile predominantly as a conjugate with glucuronic acid. This reaction takes place almost exclusively in the liver. It is the delayed expression of UGT1A1 at birth that results in an inability to access the mrp2 pump so that levels of unconjugated bilirubin-IXα rise in the liver and eventually reflux back into plasma resulting in the transiently elevated levels of bilirubin-IXα seen in neonatal jaundice. Other vertebrates; fish, birds, reptiles and amphibia excrete mainly biliverdin-IXα. Biliverdin-IXα is used for egg shell pigmentation by several bird species and also circulates, sometimes at high concentrations, in the plasma of various fish and lizards. The corollary, that these species do not express BVR-A, is not the case and we have reported studies on BVR-A from salmon [15] and *Xenopus tropicalis* [16]. Turkey red cell cytosol expresses BVR-A activity that we have partially purified on ion-exchange chromatography [17] while the chicken genome contains putative BVR-A sequences on the basis of an analysis of ESTs [18]. The basis of the difference in the biliverdin-IXα: bilirubin-IXα ratio between mammals and other vertebrates is unclear.

While the higher levels of bilirubin-IXα seen in neonatal jaundice are toxic (see below), the delayed expression of UGT1A1 may be a physiological mechanism to boost the antioxidant system at a time when the lumen of the lung is exposed to a high oxygen tension. The link between the possible antioxidant role of bilirubin-IXα and the cytoprotective role played by induction of HO-1 have stimulated studies that have recently revealed some fascinating effects of biliverdin-IXα. For example, Bach and co-workers have presented intriguing evidence that administration of biliverdin-IXα is cytoprotective for heart, colon and liver in animal transplantation studies [19, 20, 21]. In a striking report Bach and co-workers have shown that short term treatment (3 weeks) with biliverdin-IXα is sufficient to induce tolerance in a recipient to the donor heart for 120 days [21]. The introduction of an allogeneic third heart at 120 days was rejected whereas the introduction of a third syngeneic heart was accepted, clearly indicating tolerance [21]. The doses of biliverdin-IXα used in these studies are relatively high (50 μM) and require repeated administration. Co-administration of a BVR-A inhibitor (BVRI) should allow lower doses and/or less frequent administration of biliverdin-IXα, to provide cytoprotection during organ transplantation.

BVR-A is therefore a potential pharmacological target in two areas, the first in the treatment of neonatal jaundice and the second as an adjunct mechanism to allow lower doses of biliverdin-IXα to be used during organ transplantation.

Attempts to promote BVR-A as a pharmacological target have been hampered by the lack of crystal stuctures of BVR-A with bound biliverdin-IXα. Crystal structures of rat and human BVR-A complexed with NADH and $NADP^+$ respectively [22, 23] have been reported. However, without a clear definition of the biliverdin-IXα binding pocket further mechanistic studies have been severely hampered. As an alternative approach we have looked at biliverdin-IXβ reductase (BVR-B), which we have been able to crystallize (see Figure 2) with bound NADP and a number of ternary complexes with a various flavins and verdins [24]. These include (see Figure 3) the binary structure of BVR-B with

bound $NADP^+$ (PDB:1HDO) at 1.15Å resolution as well as ternary structures with bound substrates mesobiliverdin-IVα (PDB:1HE3) and flavin mononucleotide (FMN) (PDB:1HE4); and with inhibitors biliverdin IXα (PDB:1HE2) and lumichrome (PDB:1HE5). BVR-A and BVR-B share a similar short-chain dehydrogenase/reductase (SDR)-fold where the difference is largely in the extended C-terminus of BVR-A which has a "lid" over the Rossmann fold formed mainly from a β-sheet domain. Human BVR-B is a monomeric enzyme of 206 residues. It has a single domain architecture composed of a central β-sheet flanked by α-helices. The nucleotide binding fold consist of a 7 strand parallel β-sheet capped by an 8^{th} antiparallel strand and is flanked by 5 α-helices (Figure 2). The active site is made up of a further short 2-stranded parallel β-sheet, the C-terminus of helix (αE) and the flexible loops 80 and 120.

Both enzymes BVR-A and BVR-B exhibit pronounced substrate inhibition with "biliverdin" as the variable substrate (BVR-B cannot use biliverdin-IXα as a substrate, although it is a potent inhibitor) and both exhibit the same stereospecificity of hydride transfer from NADH [24, 25].

The proposed mechanism of BVR-B is suggested to be either a concerted reaction [4] or a two step mechanism (Figure 4). In principle this could involve hydride transfer from the nicotinamide C4 position to the biliverdin C10, forming a pyrrolic anion and then subsequent protonation would yield bilirubin. Alternatively, protonation of the pyrrolic nitrogen could occur first followed by hydride transfer from the nicotinamide to the C10 of a carbocation intermediate to form bilirubin. However, the exact source of the proton for these mechanisms is presently unknown. The crystal structures of BVR-B revealed the presence of a histidine residue (His153) in the active site [24]. It is proposed that His153 could act as the proton source for the "biliverdin" substrates or alternatively, the proton could be donated from bulk solvent [24].

Here we report a study in which we have used both computational and experimental approaches in order to gain insights into the BVR-B mechanism. To do this we combined a quantum mechanics/molecular mechanics (QM/MM) investigation with mutagenesis studies. Hybrid quantum mechanics/molecular mechanics (QM/MM) methods [26] are becoming an increasingly important tool for investigating the mechanisms of enzymes [27]. There are many advantages to using the QM/MM approach for modelling enzyme mechanisms. These include its ability to demonstrate catalytic functions of active site residues, identify alternate reaction intermediates and examine other important enzyme interactions, such as the role of binding residues. Using QM/MM it is possible to determine optimised transition state species, free energies for reactions and quantum effects such as tunnelling [28]. These are examples of properties that can be either difficult or impossible to measure in the wet laboratory. The transition state species of an enzyme mechanism have particular relevance for the development of new inhibitors and drug design as potent inhibitors often mimic the transition state of the enzyme.

In the present study we can define the likely mechanism as protonation of the pyrrole nitrogen atom prior to hydride transfer to the C10 position. This mechanism will probably also hold for BVR-A, which allows us to suggest that structural analogues that

cannot be protonated at the "pyrrolic" nitrogen may bind tightly without forming catalytically competent complexes and therefore function as potent biliverdin-IXα reductase inhibitors (BVRIs).

Experimental Methods

Initial rate kinetics of the wild type and H153A and H153N mutants

The initial rate kinetics with NADPH and with FMN or biliverdin-IXδ as the second substrate were conducted spectrophotometrically monitoring the rate of oxidation of NADPH at 340nm. Assays were conducted at 30°C in 100mM sodium phosphate pH 7.2 [24]. When biliverdin-IXδ was used as substrate the assay mix contained in addition 37μM BSA. Initial rate data with FMN as the second substrate were fitted to a rectangular hyperbola and the kinetic constants K_m^{NADPH}, K_m^{FMN} and k_{cat} were determined by the method of Florini and Vestling [29]. Initial rate data with biliverdin-IXδ as the variable substrate were fitted to the equation for partial substrate inhibition [30].

Computational Methods

Model building. The Michaelis complex was built using the crystal structures of BVR-B in complex with NADP(H) and the mesobiliverdin-IVα substrate as a template (PDB Code: 1HE3). The major difference between mesobiliverdin-IVα and biliverdin-IXβ are in the positions of the proprionate side chains relative to the active site of BVR-B (see Figure 5). To build the ternary complex of BVR-B with biliverdin-IXβ the A, D, C and B rings of mesobiliverdin-IVα were used as a template for the B, A, D and C rings of biliverdin-IXβ. The positioning of the side chain propionates was guided by the crystal structure of BVR-B in complex with NADP(H) and biliverdin-IXα, which has a similar propionate arrangement on the C and D pyrroles to biliverdin-IXβ (see Figure 5). The substrate was modified to biliverdin-IXβ using the QUANTA program (Accelrys). This provided us with the initial model of the BVR-B in complex with NADPH and biliverdin-IXβ.

QM/MM setup. Two different models were treated with QM/MM in the course of this investigation. The original model used His153 as the proton donor and the later model used a hydroxonium ion as the proton donor. The QM regions consisted of the imidazolium side-chain of His153 or the hydroxonium ion, rings A &D of biliverdin-IXβ and the nicotinamide moiety of NADPH. Both models included large QM regions as they required elements from the substrate, NADPH and the proton donor, therefore a link atom approach [31, 32] was applied to choose the QM regions and to treat the boundary between the QM and MM regions. Four HQ type link atoms [33] were used for QM atoms covalently bonded to MM atoms. Electrostatic, van der Waal and bonded interactions between these regions were also included. The final models and QM atom numbers are shown in Table 1. The methods used to model the QM region were the semi-empirical AM1 [34] and PM3 [35] methods. Calculations were performed using an inner unrestrained reaction region of 16Å radius with the remaining shell of the system fixed.

System preparation: All preparations were carried out using the CHARMM program [36] (version 27b2) using the CHARMM22 all-atom parameters for proteins [37] and nucleotides [38]. The system was based on a 25Å radius sphere chosen with the QM/MM simulation sphere in mind. The centre of the sphere was the oxygen of the NADPH nicotinamide ribose moiety (NO4'). Hydrogens were built onto the heavy atoms and crystallographic waters using the HBUILD function [39] in CHARMM. The system was then minimized using harmonic restraints on the mainchain and sidechains atoms of 50 and 25kcal mol^{-1} $Å^{-1}$ respectively. The system was then solvated with a pre-equilibrated 60Å cube of TIP3P model waters [40] (modified for use with CHARMM [37]). Water molecules outside the system sphere and closer than 2.8Å to existing heavy atoms were deleted. The water molecules were minimized and 10ps of equilibration MD at 300K with the protein atoms fixed. Stochastic boundary conditions [41] were applied and Langevin MD with a friction coefficient of $62ps^{-1}$ for water oxygens were used for equilibration.

Reaction modeling. The mechanisms of BVR-B were modeled by calculating a potential energy surface (PES), an approach which has been shown to perform well for other enzyme reactions [42, 43]. The PES was calculated from two reaction coordinates. The first reaction coordinate was defined as the difference of the distances between the hydride H^- from NADPH to the C^4 of the NADP(H) and the hydride H^- to the C^{10} atom of biliverdin (R1 = $d[C^4:H^-] - d[C^{10}:H^-]$). The second reaction coordinate modelled the protonation of the biliverdin pyrrole ring by His153 or a hydroxonium. The reaction coordinate was defined as the difference of the distances between the donor (histidine N^{D1}/hydroxonium O^{H2}) and acceptor N^3 to the transferring proton H^1. (R2 = $d[N^{D1}:H^1]$-$d[N^3:H^1]$ or R2 = $d[O^{H2}:H^1]$-$d[N^3:H^1]$). The PES was calculated in 0.1Å steps of the reaction coordinates using a harmonic restraint of 5000 kcal mol^{-1} $Å^{-2}$. At each step the geometry was optimized with *Adopted Basis Newton-Raphson* (ABNR) [36, 44] minimization until convergence (0.01 kcal mol^{-1} $Å^{-2}$ gradient tolerance). Atoms further than 16Å from the centre of the system were also restrained to their initial coordinates using harmonic force constants based on model *B*-factors [41].

Additional hydroxonium restraint. For some of the steps in the initial modelling of the hydroxonium donor PES, the hydroxonium was observed to donate its additional protons during the optimization. Therefore the PES was also performed using an additional harmonic restraint of 5000 kcal mol^{-1} $Å^{-2}$on the two other protons of the hydroxonium.

High-level energy corrections. Single point Density Functional Theory (DFT) corrections were performed on the final energy profile of the hydroxonium mechanisms modelled with AM1/CHARMM22 and PM3/CHARMM22. Structures generated from the two semi-empirical QM/MM potential energy surfaces were chosen and corrected using the B3LYP method with a 6-311+G* basis set. The calculations were performed using the JAGUAR [45] program version 6.0. Previous work performed with hybrid QM/MM methods has shown that corrections can be important to account for the potential shortcomings with the semi-empirical methodologies [46, 47] and have been shown to give results comparable to those observed from full *ab initio* QM/MM calculations [43, 48]. Possible pitfalls associated with energy minimisation starting from a single protein

structure have been discussed [49]. We have shown previously that an adiabatic mapping/energy minimisation approach is useful for understanding basic features of enzyme mechanisms [50, 51].

Results and Discussion

Calculations with His153 donor. Our initial observations based on the BVR-B structures [24] suggested a possible role for His153 as the proton donor for the BVR-B mechanism. The potential energy surfaces shown in Figure 6 indicate a mechanism of proton transfer followed by hydride transfer. The potential energy surfaces from both methods (AM1/CHARMM22 and PM3/CHARMM22) agree in identifying the same mechanism to be favoured. The lowest energy pathway from the biliverdin substrate (R) to bilirubin product (P) proceeds with a protonated positively charged intermediate (I^{PH}) via two transition states (TS^{PH1}, TS^{PH2}). The alternative concerted and stepwise mechanisms, of hydride transfer before proton via a negatively charged pyrrolic anion intermediate (I^{HP}), are shown to be energetically unfavourable (i.e. they have significantly higher barriers). Figure 7 shows the arrangement of the intermediate species and transition states on the QM/MM PES. The lowest energy pathway on the AM1/CHARMM22 surface has a potential energy barrier of 8.9 kcal mol^{-1} for TS^{PH1} and 20.8 kcal mol^{-1} for TS^{PH2}. The lowest energy pathway on the PM3/CHARMM22 surface has a potential energy barrier of 10.2 kcal mol^{-1} for TS^{PH1} and 13.9 kcal mol^{-1} for TS^{PH2}. The structures for the biliverdin substrate (R), the bilirubin product (P), the protonated positively charged intermediate (I^{PH}) and the two transition states (TS^{PH1}, TS^{PH2}) are shown in Figure 8.

H153A and H153N mutants. The QM/MM studies show that if His153 is the source of the proton, then a mechanism involving protonation of the pyrrole preceding hydride transfer best accords with the data. To test this hypothesis we constructed two mutants where His153 was replaced with alanine (H153A) or asparagine (H153N). This was carried out using the Stratagene "Quick Change Kit" and the mutation was verified by complete sequencing in both directions. This confirmed that the desired mutation had been achieved and that no additional mutations were introduced. Examination of the initial rate kinetics for the wild type and both H153A and H153N mutants (see Figure 9) shows clearly that His153 is not required for catalytic activity. The K_m^{NADPH} and K_m^{FMN} are modified slightly, however the k_{cat} for the H153N mutant (0.17 s^{-1}) and the H153A mutant (0.06 s^{-1}) are only slightly reduced when compared with the wild type (0.23s^{-1}). In contrast there is a significant effect on the apparent $K_m^{biliverdin\text{-}IX\gamma}$ which increases as does the substrate inhibitory apparent K_i. This result suggests that another amino acid residue or solvent water molecule must be the source of the proton. However our earlier inspection of the crystal structure suggested that His153 was the only candidate within range to donate a proton to the pyrrole nitrogen. For any other sidechain to be a candidate, considerable conformational changes in the structure would be required. The only other alternative is that the proton is received from bulk solvent. We therefore favour a model where a solvent water molecule is the source of the proton.

Calculations with hydroxonium donor. As experimentally testing the possibility of a water molecule as the proton source is difficult, we performed further QM/MM calculations to investigate this hypothesis. Preliminary calculations with neutral water as

a proton donor showed this mechanism to be unlikely, as expected. Therefore we chose to use a hydroxonium ion for further calculations. In the hydroxonium model the His153 was treated in MM as doubly protonated and charged. It was decided to keep the His153 protonated after the results of the mutagenesis experiments suggested it may still play an active role in the mechanism. In addition calculations were also performed using restraints on the protons to ensure that the hydroxonium ion did not independently donate a proton during our calculations. The tested mechanism is shown in Figure 10.

The results of the grid searches for the water donor are shown in Figure 11. The AM1/CHARMM and PM3/CHARMM surfaces for a hydroxonium ion donor infer the same mechanistic order as previously observed in the His153 surfaces. The calculated potential energy surfaces again show a clearly preferred order for the mechanism, consisting of proton transfer ($R \rightarrow I^{PH}$) from the hydroxonium to biliverdin to form a protonated cation intermediate, followed by hydride transfer to form the bilirubin product ($I^{PH} \rightarrow TS^{PH2} \rightarrow P$). However, unlike the His153 AM1/CHARMM22 PES, the mechanism does not show a transition state (TS^{PH1}) for the proton transfer from the hydroxonium ion.

The potential energy difference between the reactants (R) and intermediate (I^{PH}) was -40.5 kcal mol^{-1}. The potential energy barrier from the intermediate to the transition state (TS^{PH2}) was 17.2 kcal mol^{-1}, with an overall difference of 0.4 kcal mol^{-1} between I^{PH} and the products (P). At the intermediate state (I^{PH}) the hydride transfer distance from C^4-H' to C^{10} was 2.3Å, with an angle of attack (C^4-H'-C^{10}) of 148°. At the hydride transfer transition state (TS^{PH2}) the bond distances for C^4-H'and H'-C^{10} were 1.4Å and 1.3Å respectively and the angle of attack was 169°.

The energy profiles for the PM3/CHARMM22 method were similar to those obtained for AM1/CHARMM22. The PM3/CHARMM22 surface showed an initial large drop in energy of 36.5 kcal mol^{-1} from the starting point (R) to the intermediate (I^{PH}). The barrier to the transition state (TS^{PH2}) was 15 kcal mol^{-1} and the difference between the intermediate and product was 1 kcal mol^{-1}. The hydride transfer distance at the intermediate state (I^{PH}) C^4-H' to C^{10} was 2.3Å, with an angle of attack (C^4-H'-C^{10}) of 154°. At the transition state (TS^{PH2}) the distances for C^4-H'and H'-C^{10} were 1.3Å and 1.4Å respectively and the angle of attack was 176°. Unlike the AM1/CHARMM22 profile, the PM3/CHARMM22 profile showed a minimum state of the reactant complex that was proceeded by a small transition state barrier, indicating that a first transition state (TS^{PH1}) may still exist in the hydroxonium mechanism, in this case of 1.8 kcal mol^{-1}. The structures for the biliverdin substrate (R), the bilirubin product (P), the protonated positively charged intermediate (I^{PH}) and the two transition states (TS^{PH1}, TS^{PH2}) are shown in Figure 12.

The contributions of individual residues on the key species of the hydroxonium donor AM1/PM3//CHARMM22 surfaces are shown in Figures 13 & 14. This type of analysis allows for identification of important residues involved in stabilization of the various species [43, 52]. Figure 13 shows the average change in potential energy when each residue is removed from the systems of the key species (R,TS^{PH1},I^{PH},TS^{PH2},P) identified by QM/MM, over increasing distance from the systems centre of mass. The major

contributor in all cases was His153 and to a lesser extent His132 and Arg124. Examining the potential energy changes in the key species for these residues (Figure 14) shows His153 has the major effect on the QM region and was involved in stabilizing the intermediate (I^{PH}) the most, and the reactants (R) the least, for AM1 and PM3. Further examination of the structures showed that initially the His153 was involved in hydrogen bonding with the nicotinamide moiety of NADPH and changed conformation to hydrogen bond with the water molecule after the biliverdin was protonated.

Corrections to the hydroxonium donor PES. DFT corrections were performed for the QM regions of the structures ($R,TS^{PH1},I^{PH},TS^{PH2},P$) of the hydroxonium mechanism PES using B3LYP [53] with a 6-311+G* basis set. The corrections energy profiles descend overall (see Figure 15) agreeing with a proton before hydride transfer mechanism, with a relative ΔE of -14.9 kcal mol^{-1} (B3LYP//AM1-CHARMM22) and -19.9 kcal mol^{-1} (B3LYP//PM3-CHARMM22) for the proton transfer, and of -70.4 kcal mol^{-1} (B3LYP//AM1-CHARMM22) and -34.5 kcal mol^{-1} (B3LYP//PM3-CHARMM22) for the hydride transfer. As mentioned previously semi-empirical methods can often overestimate barriers and perform poorly for geometries and stabilities of some functional groups [46, 47]. Further work at high levels is needed to properly identify and characterise these species.

Conclusions/Revised mechanism. The use of a combined study with both experimental and computational elements has allowed valuable insights into the mechanism of BVR-B. Our experimental data and computational calculations, including analysis of the crystal structures of BVR-B, allows us to propose a revised mechanism for BVR-B. Our revised mechanism suggests firstly that the preferred pathway of the mechanism involves an initial protonation of biliverdin (R) to form an intermediate species (I^{PH}) which is followed by subsequent hydride transfer to form bilirubin (P). This reaction is highly favourable according to the methods presented in this paper. We have shown that if protonation of biliverdin is feasible, then reduction will happen efficiently in BVR-B. To demonstrate whether the mechanism is probable, further work to determine the p*K*a of the bound pyrrole is necessary.

Secondly we suggest the most likely source of proton is from bulk solvent. In addition, from our decomposition and kinetic data we propose that His153 may play an important stabilising role during the reaction, although it is not directly involved or required for catalytic activity. It is possible that the His153 is involved in the binding of the water molecule for an initial hydroxonium generation step, as observed in our structures following proton transfer to the pyrrole nitrogen the newly formed water molecule rebinds to the histidine. This could also explain our kinetics results in which theoretically the H153N would still be able to form a hydrogen bond, whereas the H153A would not. The revised mechanism is presented in Figure 16.

There are clear implications from this work for the design of inhibitors of BVR-A (BVRIs). It is likely that BVR-A will follow a similar mechanism of pyrrole protonation prior to hydride transfer. The construction of biliverdin analogs with C or S atoms replacing the "central" pyrrole N atoms should facilitate the production of compounds

that will bind tightly to BVR-A, but with no potential for reduction. The hypothetical transition states seen in Figures 8 and 12 also provide building blocks for the synthesis of transition state analogs. This work will be facilitated enormously by the solution of BVR-A structures in ternary complexes with $NADP^+$ and biliverdin.

Acknowledgements
This work was supported by a grant from Science Foundation Ireland (SFI).

References

1 Sugishima, M., Migita, C.T., Zhang, X., Yoshida, T., and Fukuyama, K. (2004) Crystal structure of heme oxygenase-1 from cyanobacterium Synechocystis sp. PCC 6803 in complex with heme. Eur. J. Biochem. **271**, 4517-4525.

2 Mantle, T.J. (2002) Haem degradation in animals and plants. Biochem. Soc. Trans. **30**, 630-633.

3 Kamisako, T., Leier, I., Cui, Y., Konig, J., Buchholz, U., Hummel-Eisenbeiss, J., and Keppler, D. (1999) Transport of monoglucuronosyl and bisglucuronosyl bilirubin by recombinant human and rat multidrug resistance protein 2. Hepatology **30**, 485-90.

4 McDonagh, A.F. (2001) Turning green to gold Nat. Struct. Biol. **8**, 198-200.

5 Foresti, R., Green, C.J., and Motterlini, R. (2004) Generation of bile pigments by haem oxygenase: a refined cellular strategy in response to stressful insults. Biochem. Soc. Symp. **71**, 177-192.

6 Ryter, S.W., Alam, J., and Choi, A.M. (2006) Heme oxygenase-1/carbon monoxide: from basic science to therapeutic applications. Physiol. Rev. **86**, 583-650.

7 Fondevila, C., Shen, X.D., Tsuchiyashi, S., Yamashita, K., Csizmadia, E., Lassman, C., Busuttil, R.W., Kupiec-Weglinski, J.W., and Bach, F.H. (2004) Biliverdin therapy protects rat livers from ischemia and reperfusion injury. Hepatology **40**, 1333-1341.

8 Sarady-Andrews, J.K., Liu, F., Gallo, D., Nakao, A., Overhaus, M., Ollinger, R., Choi, A.M., and Otterbein, L.E. (2005) Biliverdin administration protects against endotoxin-induced acute lung injury in rats. Am. J. Physiol. Lung Cell Mol. Physiol. **289**, L1131-1137

9 Kapitulnik, J. (2004) Bilirubin: an endogenous product of heme degradation with both cytotoxic and cytoprotective properties. Mol. Pharmacol. **66**, 773-779.

10 Baranano, D.E., Rao, M., Ferris, C.D., and Snyder, S.H. (2002) Biliverdin reductase: a major physiologic cytoprotectant. Proc. Natl. Acad. Sci. U S A. **99**, 16093-16098.

11 Mayer, M. (2000) Association of serum bilirubin concentration with risk of coronary artery disease. Clin. Chem. **46**, 1723-1727.

12 Vitek, L., Jirsa, M., Brodanova, M., Kalab, M., Marecek, Z., Danzig, V., Novotny, L., and Kotal, P. (2002) Gilbert syndrome and ischemic heart disease: a protective effect of elevated bilirubin levels. Atherosclerosis **160**, 449-456.

13 Lin, J.P., Cupples, L.A., Wilson, P.W., Heard-Costa, N., and O'Donnell, C.J. (2003) Evidence for a gene influencing serum bilirubin on chromosome 2q telomere: a genomewide scan in the Framingham study. Am. J. Hum. Genet. **72**, 1029-1034.

14 Stocker, R., Yamamoto, Y., McDonagh, A.F., Glazer, A.N., and Ames, B.N. (1987) Bilirubin is an antioxidant of possible physiological importance. Science **235**, 1043-1046.

15 Elliot, G. (1996) Ph.D. Thesis, University of Dublin

16 Franklin, E., Browne, S., Hayes, J., Boland, C., Dunne, A., Elliot, G., and Mantle, T. (2007) Activation of biliverdin-IXalpha reductase (BVR-A) by inorganic phosphate and related anions. Biochem. J. **405**, 61-67

17 Franklin, E. (2006) Ph.D. Thesis, University of Dublin

18 Maines, M.D. (2005) New insights into biliverdin reductase functions: linking heme metabolism to cell signaling Physiology **20**, 382-389.

19 Nakao, A., Otterbein, L.E., Overhaus, M., Sarady, J.K., Tsung, A., Kimizuka, K., Nalesnik, M.A., Kaizu, T., Uchiyama, T., Liu, F., Murase, N., Bauer, A.J., and Bach, F.H. (2004) Biliverdin protects the functional integrity of a transplanted syngeneic small bowel. Gastroenterology **127**, 595- 606.

20 Nakao, A., Neto, J.S., Kanno, S., Stolz, D.B., Kimizuka, K., Liu, F., Bach, F.H., Billiar, T.R., Choi, A.M., Otterbein, L.E., and Murase, N. (2005) Protection against ischemia/reperfusion injury in cardiac and renal transplantation with carbon monoxide, biliverdin and both. Am. J. Transplant. **5**, 282-291.

21 Yamashita, K., McDaid, J., Ollinger, R., Tsui, T.Y., Berberat, P.O., Usheva, A., Csizmadia, E., Smith, R.N., Soares, M.P., and Bach, F.H. (2004) Biliverdin, a natural product of heme catabolism, induces tolerance to cardiac allografts. FASEB J. **18**, 765-767

22 Whitby, F.G., Phillips, J.D., Hill, C.P., McCoubrey, W., and Maines, M.D. (2002) Crystal structure of a biliverdin IXalpha reductase enzyme-cofactor complex. J. Mol. Biol. **319**, 1199-1210.

23 PDB Structural Genomics Consortium 2H63

24 Pereira, P.J.B., Macedo-Ribeiro, S., Párraga, A., Pérez-Luque, R., Cunningham, O., Darcy, K., Mantle, T.J., and Coll, M. (2001) Structure of human biliverdin-IXα reductase, an early foetal bilirubin-IXβ producing enzyme. Nature Structural Biology **8** , 215-220

25 Ennis, O., Maytum, R., and Mantle, T.J. (1997) Cloning and overexpression of rat kidney biliverdin IXα reductase as a fusion protein with glutathione S-transferase: stereochemistry of NADH oxidation and evidence that the presence of the glutathione S-transferase domain does not effect BVR-A activity. Biochem. J. **328**, 33-36

27 Mulholland, A. J. (2005) Modelling enzyme reaction mechanisms, specificity and catalysis. Drug Discovery Today **10**, 1393-1402

28 Masgrau, L., Roujeinikouva, A., Johannissen, L. O., Hothi, P., Basran, J., Rana, K. E., Mulholland, A. J., Sutcliffe, M. J., Scrutton, N. S., and Leys, D. (2006) Atomic Description of an Enzyme Reaction Dominated by Proton Tunneling. Science **312** (5771), 237-241

29 Florini, J. R., and Vestling, C. S. (1957) Graphical determination of the dissociation constants for two-substrate enzyme systems. Biochimica Biophysica Acta. **25**, 575-578

30 Phillips, M. F., and Mantle, T. J. (1991) The initial-rate kinetics of mouse glutathione S-transferase YfYf. Evidence for an allosteric site for ethacrynic acid. Biochemical Journal **275**, 703-709

31 Singh, U. C., and Kollman, P. A. (1986) A combined ab initio QM/MM method for carrying out simulations on complex systems: Application to the $CH_3Cl + Cl^-$ exchange reaction and gas phase protonation of polyethers. J. Comp. Chem. **7**, 718-730

32 Antes, I., and Thiel, W. (1998) On the Treatment of Link Atoms in Hybrid Methods. In: Gao, J., and Thompson, M. A. (eds). Combined Quantum Mechanical and Molecular Mechanical Methods, American Chemical Society, Washington D.C.

33 Reuter, N., Dejaegere, A., Maigret, B., and Karplus, M. (2000) Frontier Bonds in QM/MM Methods: A Comparison of Different Methods. J. Phys. Chem. A **104**, 1720-1735

34 Dewar, M. J. S., Zoebisch, E. G., Healy, E. F., and Stewart, J. J. P. (1985) AM1: A New General Purpose Quantum Mechanical Molecular Model. J. Am. Chem. Soc. **107**, 3902-3909

35 Stewart, J. J. P. (1989) Optimization of parameters for semi-empirical methods. I. Method. J. Comp. Chem. 10(2), 209-220

36 Brooks, B. R., Bruccoleri, R. E., Olafson, B. D., States., D. J., Swaminathan, S., and Karplus, M. (1983) CHARMM: A Program for Macromolecular Energy, Minimization, and Dynamics Calculations. J. Comp. Chem. **4**(2), 187-217

37 MacKerell, A. D., Bashford, D., Bellott, M., Dunbrack, R. L., Evanseck, J. D., Field, M. J., Fischer, S., Gao, J., Guo, H., Ha, S., Joseph-McCarthy, D., Kuchnir, L., Kuczera, K., Lau, F. T. K., Mattos, C., Michnick, S., Ngo, T., Nguyen, D. T., Prodhom, B., Reiher, W. E., Roux, B., Schlenkrich, M., Smith, J. C., Stote, R., Straub, J., Watanabe, M., Wiorkiewicz-Kuczera, J., Yin, D., and Karplus, M. (1998) All-atom empirical potential for molecular modeling and dynamics studies of proteins. J. Phys. Chem. **102**, 3586-3616

38 Pavelites, J. J., Gao, J. L., Bash, P. A., and Mackerell, A. D. (1997) A molecular mechanics force field for NAD(+), NADH, and the pyrophosphate groups of nucleotides. J. Comp. Chem. **18**(2), 221-239

39 Brunger, A. T., and Karplus, M. (1988) Polar hydrogen positions in proteins: Empirical energy placement and neutron diffraction comparison. Proteins-Structure Function and Genetics **4**, 148-156

40 Jorgensen, W. L., Chandrasekhar, J., Madura, J. D., Impey, R. W., and Klein, M. L. (1983) Comparison of simple potential functions for simulating liquid water. J. Chem. Phys. **79**, 926-935

41 Brooks, C. L., and Karplus, M. (1989) Solvent effects on protein motion, and protein effects on solvent motion. Dynamics of the active site region of lysozyme. J. Mol. Biol. **208**, 159-181

42 Hermann, J. C., Ridder, L., Mulholland, A. J., and Holtje, H. D. (2003) Identification of Glu166 as the general base in the acylation reaction of class A beta-lactamases through QM/MM modeling. J. Am. Chem. Soc. **125**, 9590-9591

43 Hermann, J. C., Hensen, C., Ridder, L., Mulholland, A. J., and Holtje, H. D. (2005) Mechanisms of Antibiotic Resistance: QM/MM Modeling of the Acylation Reaction of a Class A β-Lactamase with Benzylpenicillin. J. Am. Chem. Soc. **127**, 4454-4465

44 Boyd, R. H. (1968) Method for calculation of the the conformation of minimum potential-energy and thermodynamic functions of molecules from empirical Valence-force potentials – application to the cyclophanes. J. Chem. Phys. **19**, 2574

45 Jaguar version 6.0. In., Schrödinger, LLC, New York, NY, 2005.

46 Jensen, F. (1999) Introduction to Computational Chemistry. John Wiley & Sons Ltd.

47 Leach, A. R. (2001) Molecular Modelling Principles and Applications, 2nd Edition Ed., Personal Education Limited.

48 Ranaghan, K. E., Ridder, L., Szefczyk, B., Sokalski, W. A., Hermann, J. C., and Mulholland, A. J. (2004) Transition state stabilization and substrate strain in enzyme catalysis: *ab initio* QM/MM modelling of the chorismate mutase reaction. Organic & Biomolecular Chemistry. **2**, 968-980

49 Klähn, M., Braun-Sand, S., Rosta, E., and Warshel, A. (2005) On possible pitfalls in ab initio quantum mechanics/molecular mechanics minimization approaches for studies of enzymatic reactions. J. Phys. Chem. B. **109**:15645-50.

50 Lodola, A., Mor, M., Hermann, J.C., Tarzia, G., Piomelli, D., and Mulholland A.J. (2005) QM/MM modelling of oleamide hydrolysis in fatty acid amide hydrolase (FAAH) reveals a new mechanism of nucleophile activation. Chem. Commun. (Camb.) (35):4399-4401.

51 Claeyssens, F., Harvey, J.N., Manby, F.R., Mata, R.A., Mulholland, A.J., Ranaghan, K.E., Schütz, M., Thiel, S., Thiel, W., and Werner H.J. (2006) High-accuracy computation of reaction barriers in enzymes. Angew. Chem. Int. Ed. Engl. **45**:6856-9.

52 Ridder, L., Rietjens, I. M. C. M., Vervoort, J., and Mulholland, A. J. (2002) Quantum Mechanical/Molecular Mechanical Free Energy Simulations of the Glutathione S-Transferase (M1-1) Reaction with Phenanthrene 9,10-Oxide. J. Am. Chem. Soc **124**, 9926-9936

53 Becke, A. D. (1993) Density-Functional Thermochemistry. III. The Role of Exact Exchange. J. Chem. Phys. **98**, 5648

Legends to Figures

Figure 1 **Chemical structures of biliverdin-IXβ and bilirubin-IXβ**

Figure 2 **Human BVR-B with bound $NADP^+$**

Figure 3 **Ternary complexes of BVR-B**. The Figure shows BVR-B with bound $NADP^+$ and a) biliverdin-IXα, b) mesobiliverdin-IVα, c) flavin mononucleotide and d) lumichrome

Figure 4 **Proposed mechanisms for BVR-B**. The proposed concerted and two step mechanism are illustrated.

Figure 5 **Chemical structures of bound biliverdins**. The structures of the two verdins for which there are ternary complex structures (mesobiliverdin-IVα and biliverdin-IXα) are shown together with the structure for biliverdin-IXβ in panel a). In panel b) these are idealised as cartoons to illustrate the orientation of the four pyrrole rings in the active site together with the various orientations of the two proprionate side chains. The top and bottom cartoons of panel b) have NADPH adjacent to the reducible C10, while in the middle panel the linear tetrapyrrole is rotated 90˚ so that the C-10 position is too far from the C4 of NADPH to accept a hydride.

Figure 6 **Potential energy surfaces for the BVR-B reaction with His153 as the proton donor.** These are shown for; (a) AM1/CHARMM22 and (b) PM3/CHARMM22. The key species noted are identified in the mechanism shown in Figure 7

Figure 7 **The nature of the key species identified in the QM/MM potential energy surfaces**. The two transition states and ionic intermediates are labelled as PH (protonation followed by hydride transfer) or HP (hydride transfer followed by protonation). The proton Donor is either His153 (Figure 8) or hydroxonium (Figure 12).

Figure 8 **Structures from modelling the BVR-B reaction with His153 as proton donor**. This shows the key groups; biliverdin-IXβ, His153 sidechain and nicotinamide moiety of the preferred protonation followed by hydride transfer mechanism from modelling with AM1/CHARMM22.

Figure 9 **Initial rate kinetics for wild type and H153A and H153N mutants.** Initial rates are plotted against the indicated concentrations of NADPH with the following concentrations of FMN: 10μM (▲), 20μM (♦), 50μM (■), 100μM (□) and 150μM (◊). Assays were performed in 100mM

potassium phosphate, pH 7.5 at 30°C. Date is shown for the (a) wild type [35μg], (b) H153N [45μg] and (c) H153A [47μg]. All data points represent the mean of triplicate determinations (+/- SE of the mean). The solid lines are least squares fits to a rectangular hyperbola.

Fig. 10 **BVR-B mechanism with alternative proton donors**. Panel (a) shows the mechanism with His153 as the proton donor and panel (b) with hydroxonium as the proton donor.

Figure 11 **Potential energy surfaces for the BVR-B reaction with hydroxonium as proton donor.**

Figure 12 **Structures from modelling the BVR-B reaction with hydroxonium as proton donor**. This shows the key groups; biliverdin-IXβ, His153 sidechain, hydroxonium and nicotinamide moiety of the preferred protonation followed by hydride transfer mechanism from modelling with AM1/CHARMM22.

Figure 13 **Average contribution of MM residues to QM/MM interaction energy**. This shows the average contribution of individual residues for key species in the BVR-B mechanism modelled with (●) AM1/CHARMM22 and (▲) PM3/CHARMM22.

Figure 14 **Change in MM contribution over the course of the BVR-B hydroxonium donor mechanism**. This shows the change in contributions made by the residues His153 ((■) AM1/ (□) PM3), Arg124 ((●)AM1/ (○) PM3) and His132 ((▲)AM1/ (Δ) PM3), for both AM1/CHARMM22 and PM3/CHARMM22 as the reaction progresses.

Figure 15 **B3LYP/6-311+G*//AM1/CHARMM22 and B3LYP/6-311+G*//PM3/CHARMM22 corrected energies, relative to R, for the hydroxonium donor mechanism.** This shows B3LYP/6-311+G*//AM1/CHARMM22 (●) and B3LYP/6-311+G*//PM3/CHARMM22 corrected energies (▲), relative to R.

Figure 16 **Proposed revision to the BVR-B mechanism in which a proton transfer is followed by hydride transfer via the transition species noted.**

Table 1 **Table of components and atoms in His153 and hydroxonium QM/MM system.**

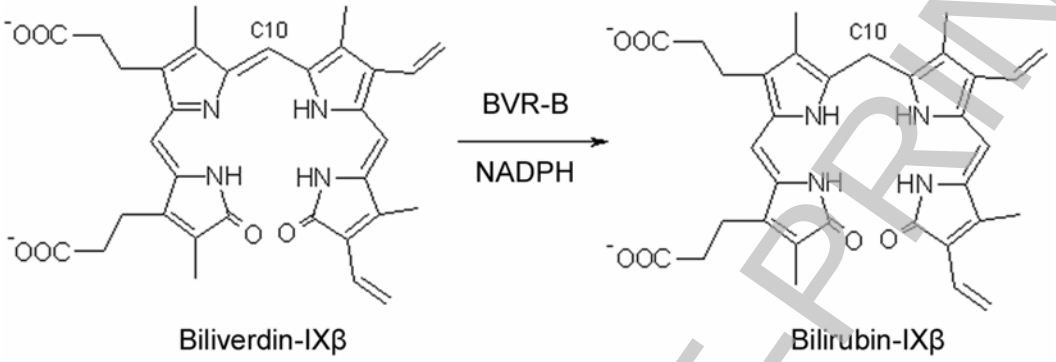

Figure 1

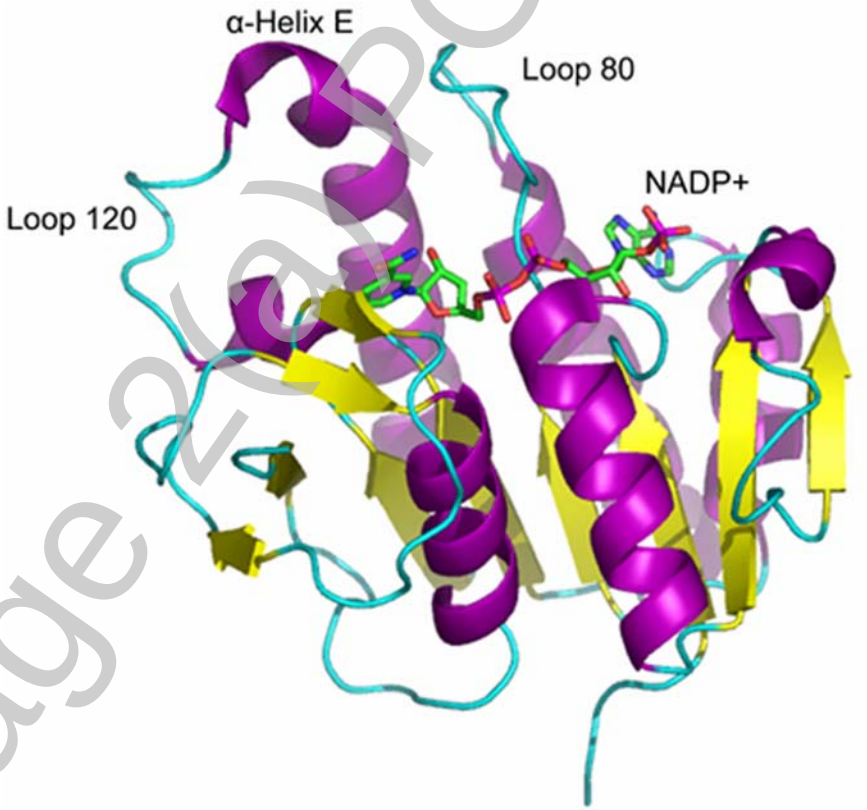

Figure 2

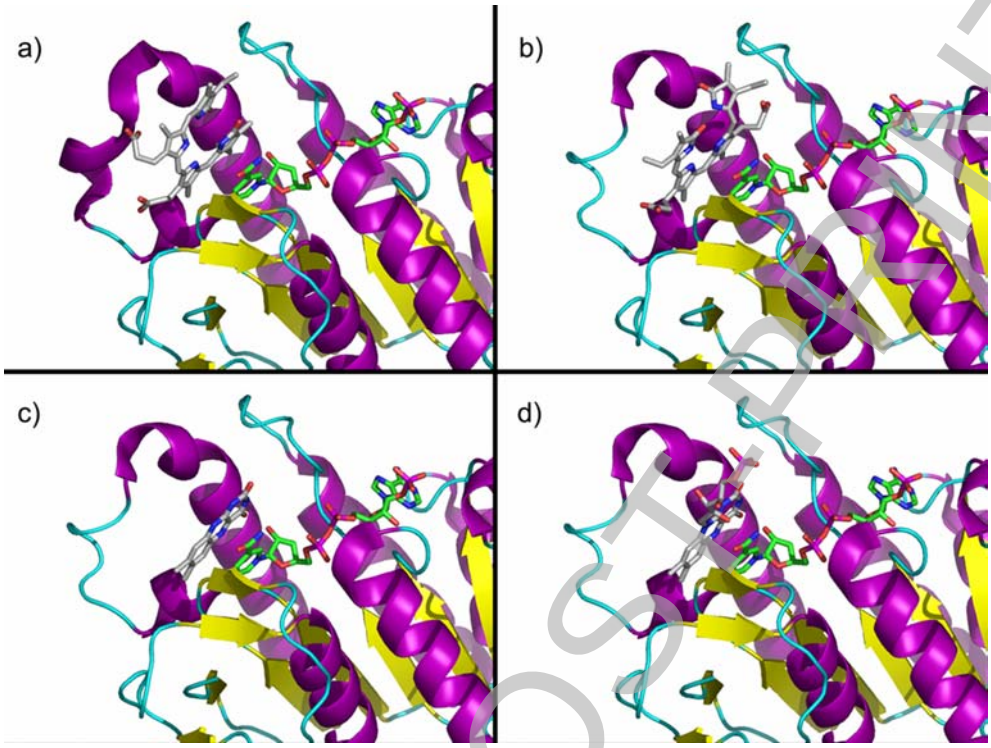

Figure 3

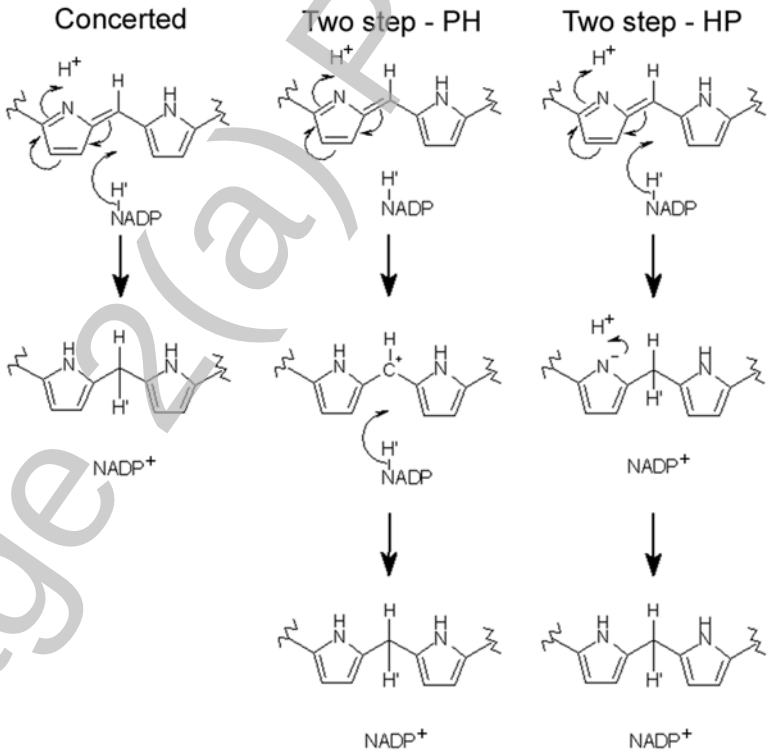

Figure 4

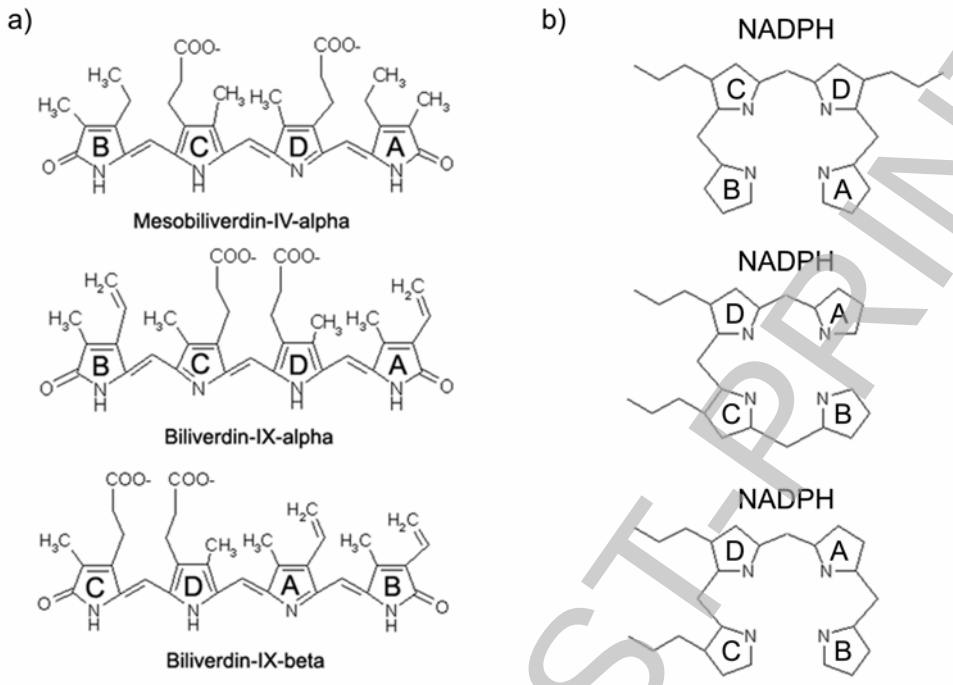

Figure 5

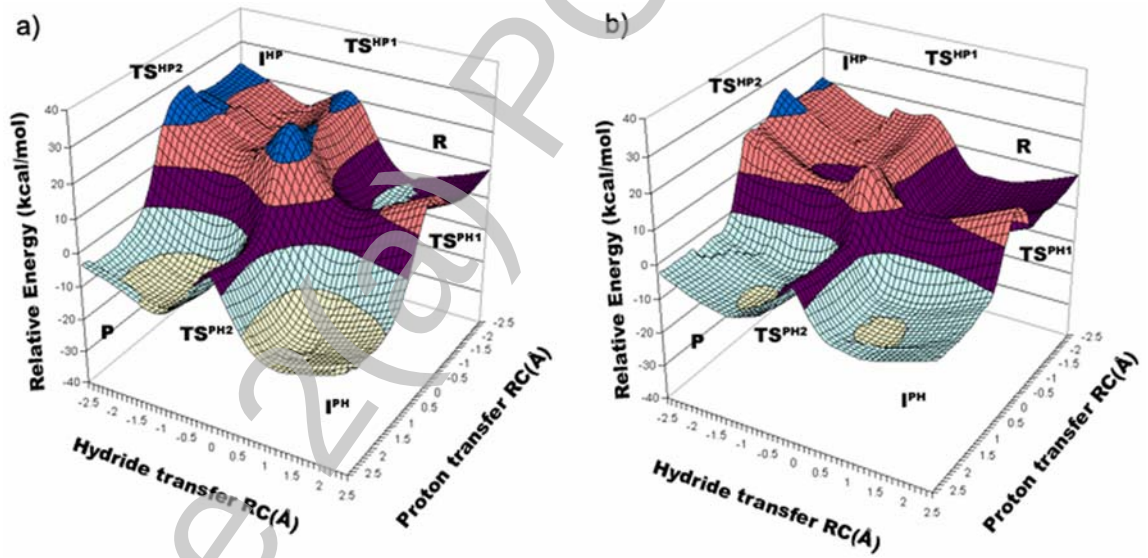

Figure 6

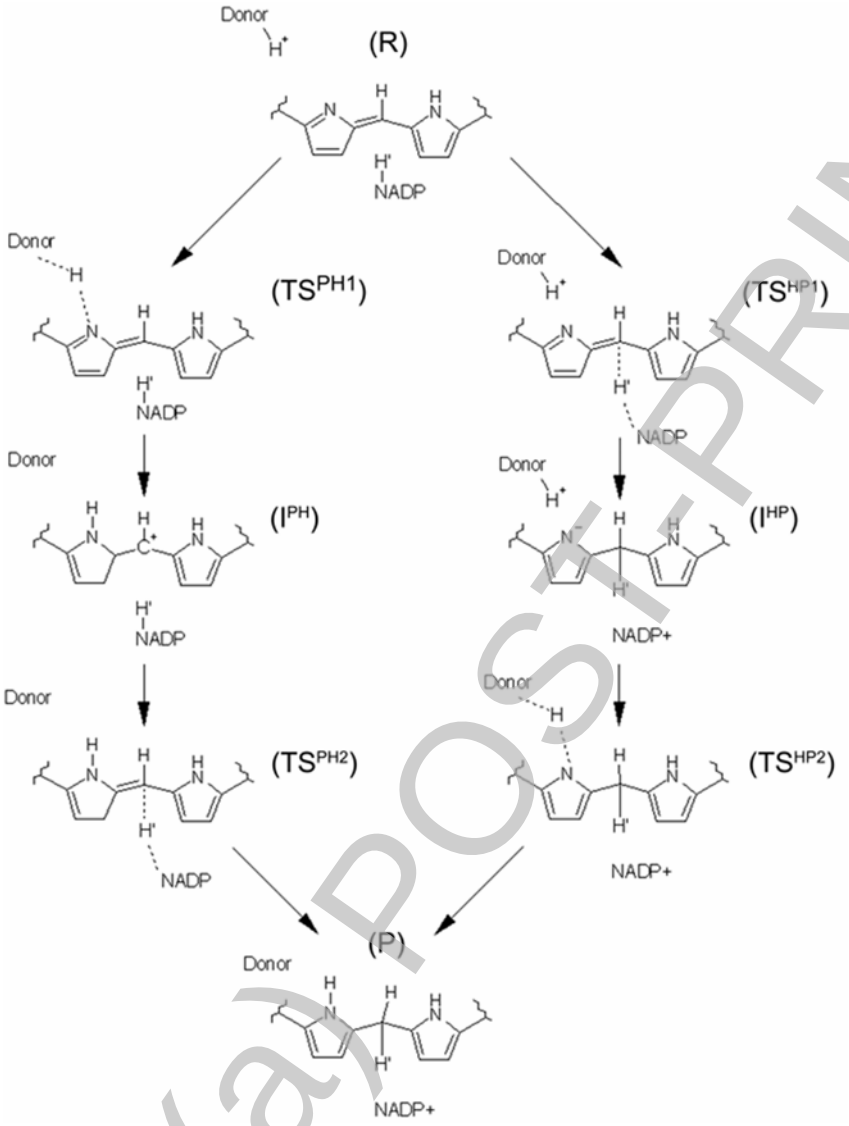

Figure 7

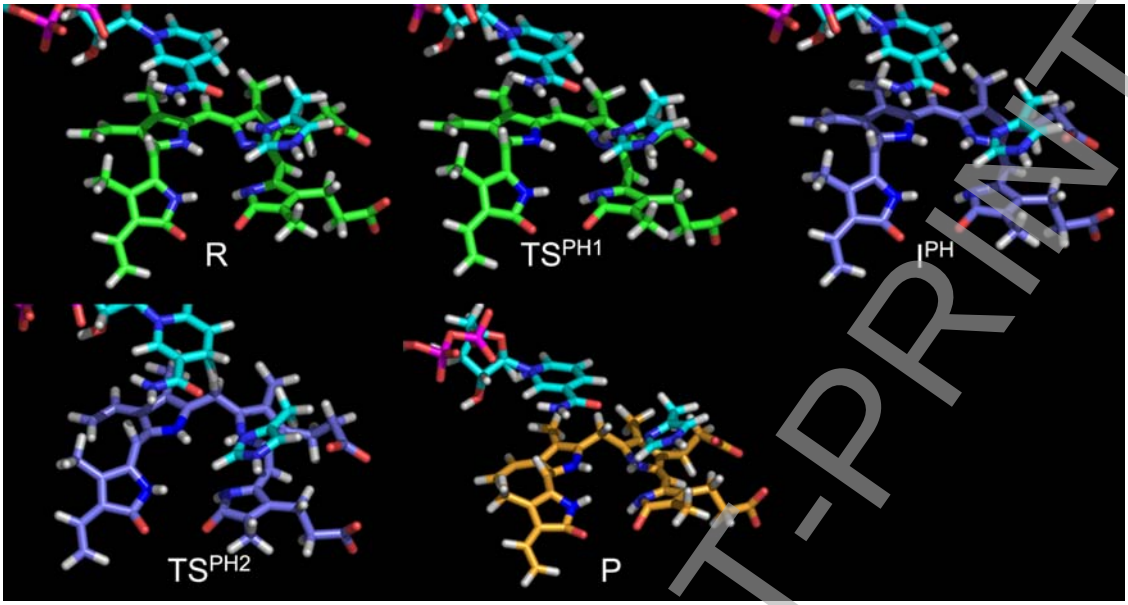

Figure 8

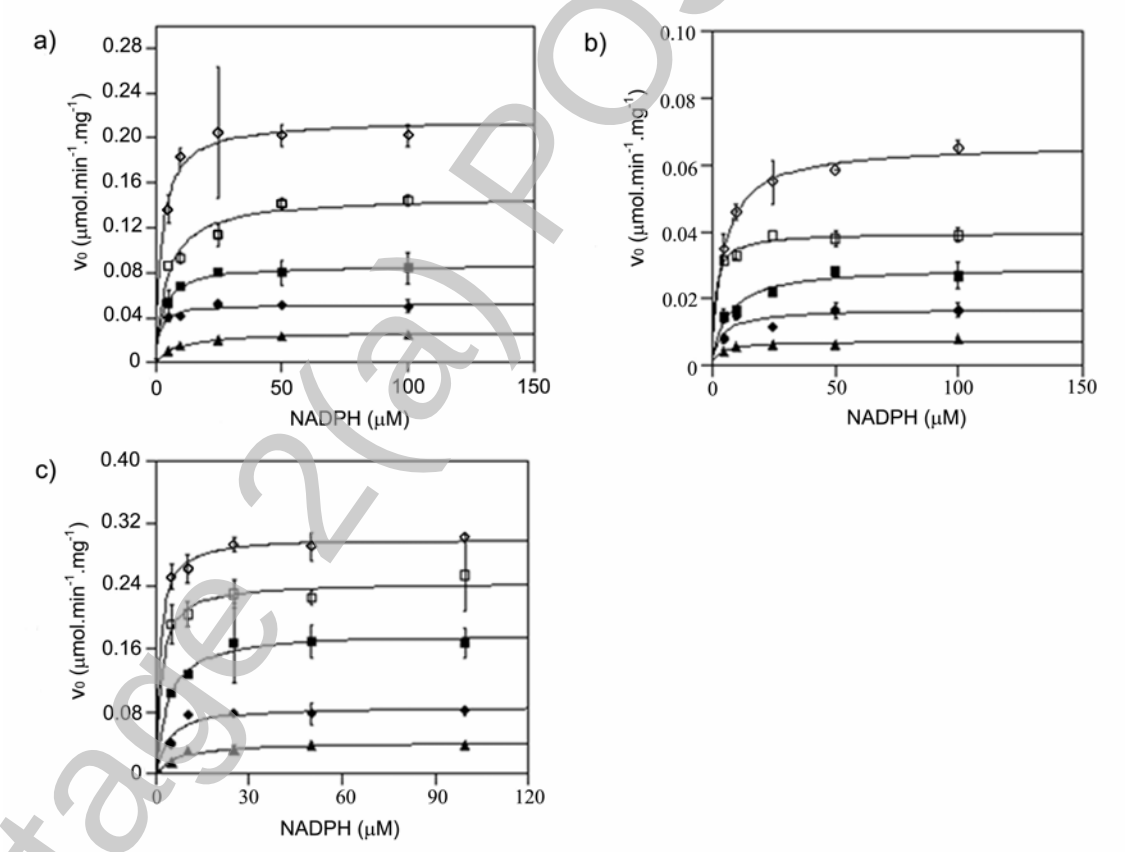

Figure 9

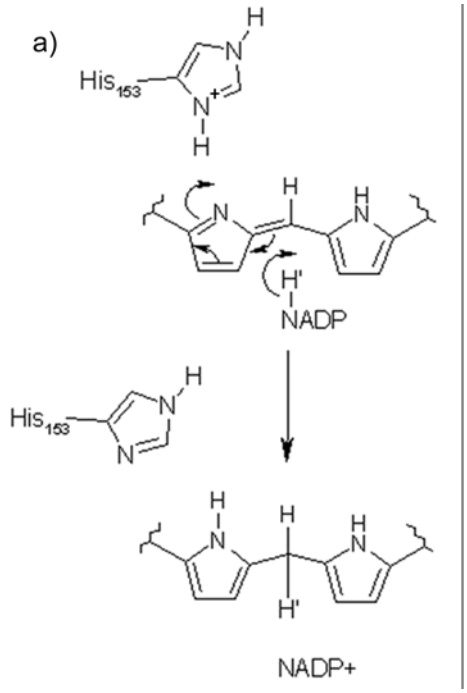

Figure 10

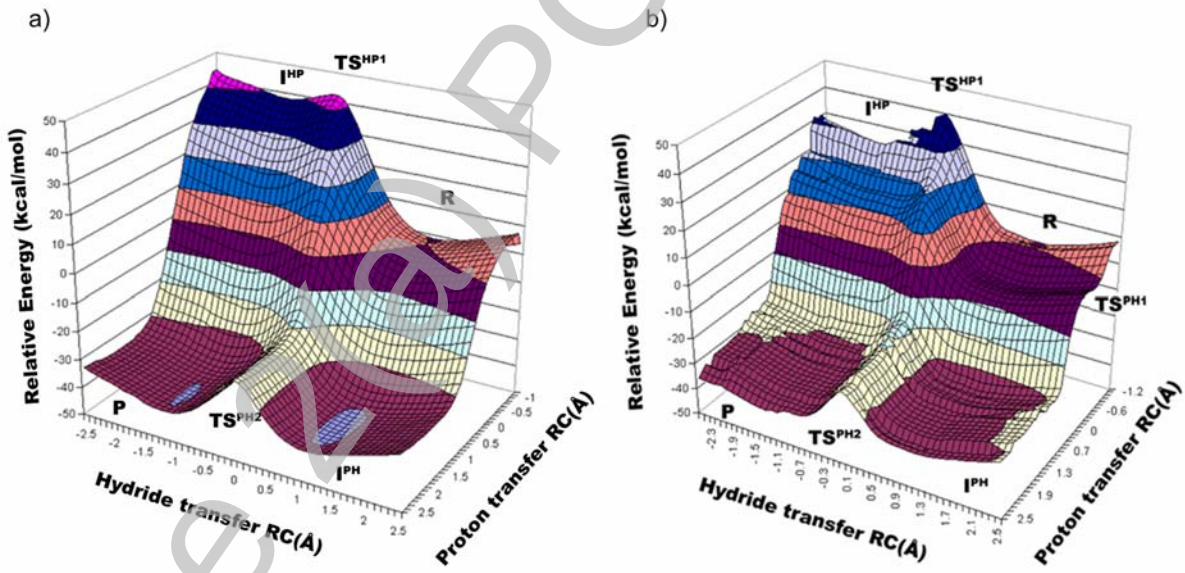

Figure 11

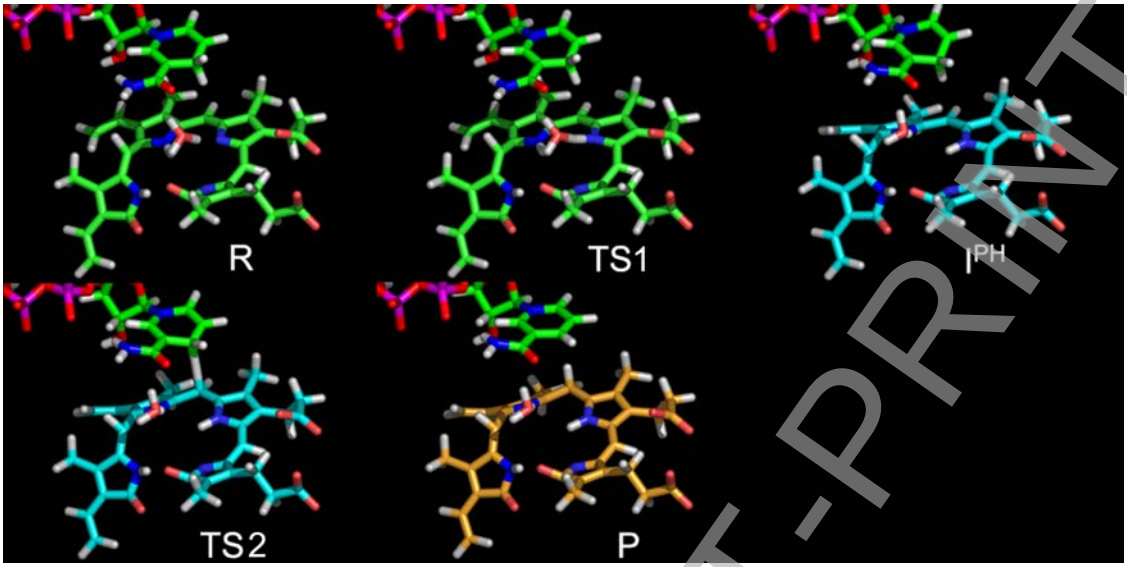

Figure 12

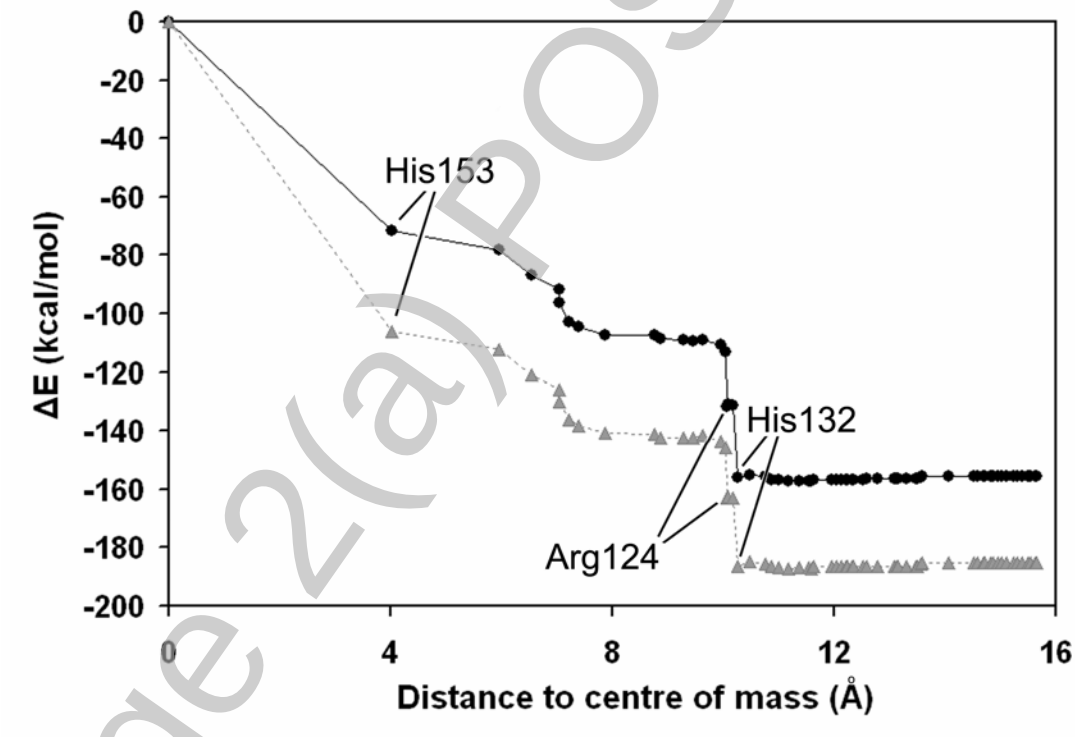

Figure 13

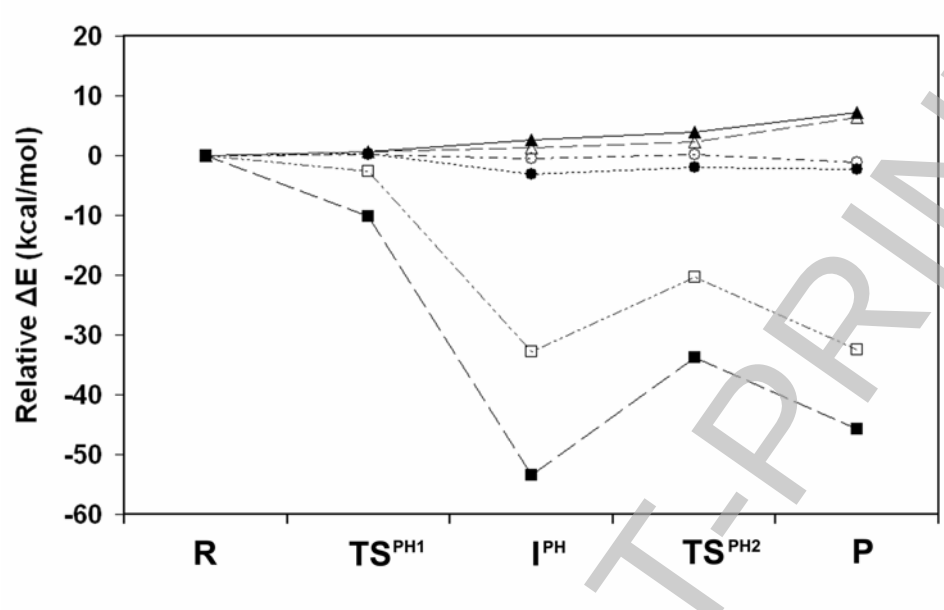

Figure 14

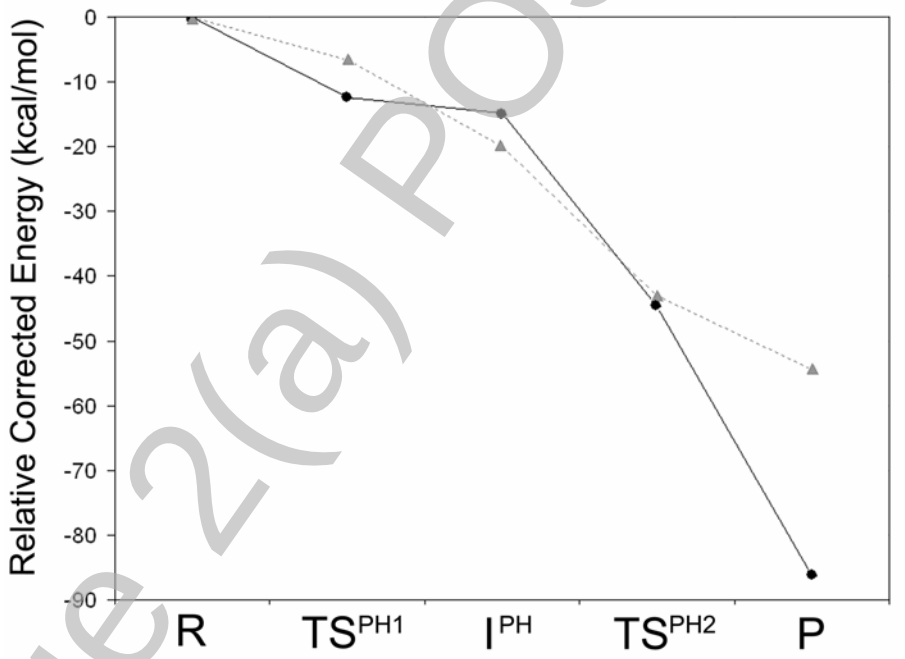

Figure 15

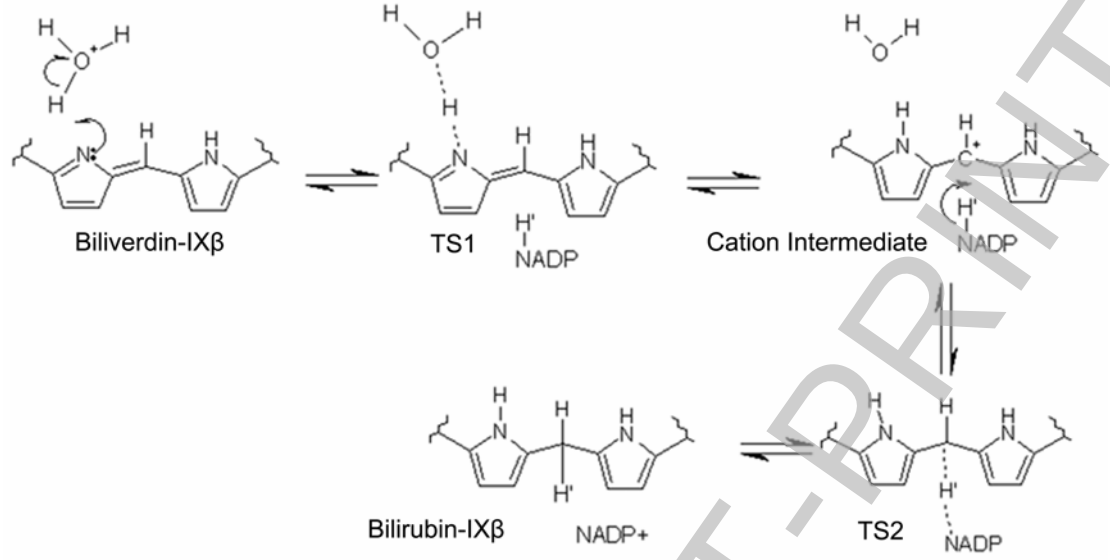

Figure 16

System	His153 donor	Hydroxonium donor
Components		
Residues	200	200
Water molecules	1119	1119
Atoms		
MM region	6493	6502
QM region	67	58
Total atoms	6560	6560

Table 1